Colloids and Surfaces A: Physicochemical and Engineering Aspects 697 (2024) 134319

Contents lists available at ScienceDirect

Colloids and Surfaces A: Physicochemical and Engineering Aspects

journal homepage: www.elsevier.com/locate/colsurfa

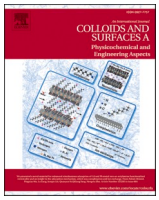

Direct force measurements between sub-micron rod-shaped colloids by AFM

S. Sittl [a], M. Das [b,c], N. Helfricht [a,d], G. Petekidis [b,c,*], G. Papastavrou [a,d,**]

[a] Physical Chemistry II, University of Bayreuth, Bayreuth 95447, Germany
[b] IESL-FORTH, Heraklion GR-71110, Greece
[c] Department of Material Science and Technology, University of Crete, Heraklion GR-71110, Greece
[d] Keylab Surface and Interface Characterization, Bavarian Polymer Institute, University of Bayreuth, Bayreuth 95447, Germany

GRAPHICAL ABSTRACT

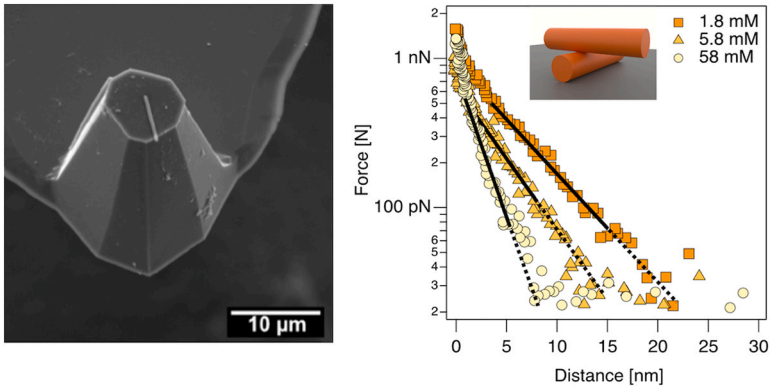

ARTICLE INFO

Keywords:
AFM
Direct force measurements
DLVO
Colloidal systems

ABSTRACT

The colloidal probe (CP) technique is an essential tool for quantitative direct force measurements by atomic force microscopy (AFM). By attaching a colloidal particle to the free end of an AFM-cantilever, not only a defined interaction geometry can be accomplished, but also a nearly arbitrary surface chemistry becomes possible. Commonly, the CP-technique is utilized for spherical particles in the sphere/sphere or sphere/plane interaction geometry. Here, the CP-technique has been extended to rod-shaped colloids with diameters well below one micrometer, thus preparing 'rod probes' based on a procedure similar to that known from DNA combing, allowing for a controlled alignment between these rods and the rod probe. In combination with AFM-imaging by the rod on the probe, sufficiently orthogonally aligned pairs of rods can be identified, and direct force measurements in the crossed-cylinder geometry, similar to the surface force apparatus (SFA), can be accomplished. A proof-of-concept of direct force measurements between silica rods with diameters of 270 ± 50 nm has been presented. The acquired interaction force profiles have been quantitatively evaluated within the framework of the full solutions of the Poisson-Boltzmann equation, including charge regulation.

* Corresponding author at: IESL-FORTH, Heraklion GR-71110, Greece.
** Corresponding author at: Physical Chemistry II, University of Bayreuth, Bayreuth 95447, Germany.
E-mail addresses: georgp@iesl.forth.gr (G. Petekidis), georg.papastavrou@uni-bayreuth.de (G. Papastavrou).

https://doi.org/10.1016/j.colsurfa.2024.134319
Received 18 February 2024; Received in revised form 16 May 2024; Accepted 21 May 2024
Available online 3 June 2024

1. Introduction

In the last three decades, the atomic force microscope (AFM) developed from a tool primarily used for imaging purposes to a very versatile analytical instrument that also allows for the direct determination of surface forces [1–3]. Previously, such direct force measurements have been the domain of the surface force apparatus (SFA). The development of quantitative force measurements by AFM has been substantially facilitated by the introduction of the colloidal probe (CP) technique, which was independently presented by Ducker [3] and Butt [4]. This technique is based on attaching a colloidal particle to the free end of an AFM-cantilever, thereby replacing the sharp tip with a colloid of exchangeable surface chemistry and defined interaction geometry [5–7]. Various types of colloidal particles have been utilized in the past as probes, ranging from hard inorganic materials (e.g., glass or silica particles) [3,4,8–10] or organic materials (e.g., polystyrene particles) [11–13] to soft materials, such as hydrogel beads [8]. However, nearly all measurements reported by the colloidal probe technique were performed with spherical probes [5–7] with few exceptions [9–17]. However, the great advantage of the colloidal probe technique is that it allows, in principle, to utilize every type of colloidal object as a probe, including cylindrical rod-shaped particles.

Recently, rod-shaped colloids have received much attention as they allow for the preparation of anisotropic materials, e.g., in order to control heat flow or fluid viscosity [18–20]. Concentrated colloidal suspensions of non-spherical particles also provide interesting additional degrees of freedom to tune gel properties with a significant influence of particle shape on the resulting rheological properties [21,22]. Moreover, the adsorption kinetics of non-spherical particles to planar substrates provide important insights for the adsorption of non-spherical objects, such as proteins [23,24]. The fundamental understanding of the governing interaction forces is essential for all these different colloidal systems. Hence, developing approaches that allow for direct force measurements of such non-spherical colloids would be necessary as these anisotropic particles are commonly significantly smaller than the other non-spherical objects used so far as colloidal probes [6,7,25]. The importance of directly measuring interaction forces in order to understand phenomena such as aggregation for colloidal suspensions has been pointed out in the past [26,27]. We predict, that in the case of anisotropic particles the importance of understanding the govering interaction force might have even more benefits.

Here, we present a new approach to determining interaction forces between rod-shaped colloidal particles with diameters of about 300 nm. By classical definition, such colloidal rods cannot be considered as ‘nanorods’, albeit their diameter is significantly less than a micron. There is an analogy to the term ‘nanoparticle’, which is commonly reserved for particles with diameters less than 100 nm [28]. To the best of our knowledge, no direct force measurements of such small rod-shaped colloids have been reported so far. It should be highlighted that only a small number of direct force measurements have been reported with spherical colloidal particles bearing diameters smaller than 1 μm [25,29–31]. In the case of cylindrical objects, such as rods, the so-called crossed cylinder geometry provides a well-defined interaction geometry that is identical to the one of the SFA [32,33]. This interaction geometry can be described by the Derjaguin approximation, which is similar to the interaction between spherical particles [32–34].

In order to determine quantitatively the interaction forces between rod-shaped colloids with sub-μm diameters, several experimental challenges have to be addressed: First, the geometric constraints due to the attachment of the rods on flat surfaces pose boundary conditions for the immobilization on the substrate as well as on the cantilever. Second, the force contributions by the lever arm must be excluded as its area is large compared to that of the rod. Third, one has to ensure a defined relative position between two rods, which are not visible by optical microscopy, in order to achieve the crossed-cylinder geometry. For all these fundamental impediments, we have been able to find experimental solutions and can present a proof-of-concept for quantitative direct force measurements between two rod-shaped colloids in a defined interaction geometry.

2. Materials and methods

2.1. Synthesis

The rod-shaped silica particles have been prepared according to a protocol described in the literature [35]. The synthesis and the analytical outcome have been reported previously [22]. Briefly: De-ionized (DI) water, obtained from a Millipore apparatus with a resistivity of 18.2 Ω.cm at 298 K, was used for the rod synthesis. 12 g of polyvinylpyrrolidone 40k (PVP, Aldrich) were dissolved in 1.2 L 1-pentanol (98 %, Alfa Aesar) by sonication for 3 h. Next, 32.4 mL DI water, 7.2 mL of 0.18 M sodium citrate (sodium citrate dihydrate, 99 %, Aldrich) solution and 128 mL ethanol (98 %, Alfa Aesar) were added and the reaction medium was mixed with an overhead stirrer for 5 min. 24.3 mL ammonium hydroxide solution (25 wt%, Aldrich) and 10.8 mL of tetraethyl orthosilicate (TEOS, 98 %, Aldrich) were added before stirring for 60 s. After 4 h, 5.4 mL of TEOS were added, and the mixture was shaken by hand. The reaction was left to proceed overnight without stirring. The rods were recovered by centrifugation at 4400 g for 1.5 h, and washed by centrifugation/re-dispersion cycles: 4 times in ethanol at 736 g, 4 times in water at 736 g, 8 times in water at 304 g. The supernatants of the centrifugation cycles were discarded, to remove the smaller rods, and the precipitates were retained. The larger rods or aggregates were removed by two additional centrifugation cycles in DI water at 60 g by discarding the precipitates and retaining the supernatant. The rods were recovered from the supernatant by centrifuging at 2500 g for 20 min.

2.2. Conductivity of electrolyte solutions

The conductivities of the electrolyte solutions were determined with a combined pH/Conductometer (914 pH/Conductometer, Metrohm, Herisau, Switzerland). Before the measurements, a calibration of the conductometer was carried out with conductivity standards (100 μS/cm KCl in water, Metrohm, Herisau, Switzerland).

2.3. Characterization of nanorods by atomic force microscopy (AFM) and scanning electron microscopy (SEM)

AFM-images of the drop casted rod-shaped colloids were acquired with a Dimension Icon AFM (Bruker Corporation Billerica, Massachusetts, USA) equipped with a NanoScope V controller. For imaging purposes, standard tapping mode cantilevers (OMCL-AC160TS, Olympus, Japan) were used. The tapping mode frequency was set to 95 % of the cantilever’s actual resonance frequency with an excitation amplitude of 500 mV and an amplitude setpoint of about 400 mV. The AFM images were processed with NanoScope Analysis software (version 1.80).

For scanning electron microscopy imaging, the substrates or cantilevers were sputtered with a 1.5 nm platinum layer (Cressington Platin-Sputter Coater 208 HR, Tescan GmbH, Dortmund, Germany) and imaged by SEM (FEI Quanta FEG 250, Thermo Fischer, Waltham, Massachusetts, USA). For the images using the secondary electron detector were acquired at a working distance of 5 mm with an acceleration voltage of 15 kV.

2.4. Combing of rod-shaped colloids on substrates

Glass disks (Irlbacher Blickpunkt Glas GmbH, Germany) were cleaned by an expanding CO_2-treatment using a SnowJet (Applied Surface Tecnologies, New Jersey, USA), followed by 20 minutes of exposure to air plasma (Zepto, Diener Electronics, Ebhausen, Germany). Subsequently, 50 μL of a 0.01 wt% suspension of the colloidal rods was placed

at the edge of the glass disk. A nitrogen stream with a pressure of 4 bar was applied at an angle of 0° with respect to the substrate's surface, until the glass substrate was dry. The success of the alignment was routinely evaluated using optical microscopy with 40x magnification (Axio Examiner.D1, Zeiss, Oberkochen, Germany).

2.5. Preparation of rod probes on AFM cantilevers

Cantilevers with a plateau tip (SD-PL-CONT-10, nominal spring constant: 0.2 N/m, Nanosensors, Neuchatel, Switzerland) were cleaned by air plasma treatment (Zepto, Diener Electronic, Ebhausen, Germany). Rod shaped colloids were attached to the cantilever via a micromanipulation process similar to the one reported previously for spherical silica particles [36]. This process results in a permanent immobilization of the rod-shaped colloids to the cantilever, in difference to aspiration techniques based on fluidic force microscopy [30,31]. An etched tungsten wire was used to place a tiny droplet of UV-curing glue (NOA63, Norland Adhesives) on the plateau tip with the help of a motorized micromanipulator (DC-3 K, Märzhäuser, Wetzlar, Germany). Subsequently, a rod-shaped colloid was placed onto the droplet with another tungsten wire. The amount of glue was sufficiently small in order to prevent wetting of the rod. The process has been monitored on a fixed-stage optical microscope (Axio Examiner.D1, Zeiss, Oberkochen, Germany) to which the micromanipulator has been attached. Subsequently the etched tungsten wire used for manipulating the glue has been exchanged for a fresh wire, which has then been used to pick-up a single rod-shaped particle and holding it only by capillary forces. By placing this rod in the previously prepared glue spot, the adhesion of the latter was stronger than for the capillary forces. Curing has been carried out by a mercury lamp. After attaching the rod, the spring constant was calibrated by the thermal noise method [37].

2.6. In-situ imaging with rod-probes and direct force measurements

All AFM imaging and force distance measurements using the rod-probes were performed on a commercial AFM system (Nanowizard 4, JPK BioAFM, Berlin, Germany). The AFM was mounted on an inverted optical microscope (Axiovert 200, Zeiss, Oberkochen, Germany) in order to monitor the cantilever as well as the substrate. The experiments were performed in a commercial fluid cell (Asylum Research, Oxford Instruments, Abingdon, UK), into which circular glass disks (Irlbacher Blickpunkt Glas GmbH, Germany) were mounted. Imaging of the adsorbed rods was then performed in QI-Mode.

After the identification of suitable rods by imaging, direct force measurements were carried out by ramping the z-piezo in the 'point and shoot' method, selecting specific points in the images. For each ionic strength, a new substrate of pre-aligned rods was prepared. In between changes of the ionic strength, the cantilever has been rinsed with Milli-Q water to remove salt residues. Measurements were performed on different spots on each rod, on each spot at least 50 measurements. For each ionic strength, at least two rod combinations were probed.

2.7. Quantitative evaluation of force measurements

The raw data were exported with the JPK Image Processing Software 6.1.169 (JPK BioAFM, Berlin, Germany) and subsequently converted into a plot of force versus displacement in a custom-written procedure with IgorPro (Wavemetrics, Nimbus, Portland, USA). A script was used to fit the exponential decay, in the interval $0.5\kappa^{-1}$ to $2\kappa^{-1}$ of the Debye length κ^{-1} for 1.8 mM and 5.8 mM, respectively. The data measured at an ionic strength of 58 mM were fitted between $1\kappa^{-1-1}$ and $2\kappa^{-1}$.

Symmetric fits to the full solutions of the Poisson-Boltzmann were performed by fixing the regulation parameter p to 0.6 and fitting the diffuse layer potential as well as the ionic strength with custom software [38]. These fits were performed between $0.5\kappa^{-1}$ - $2\kappa^{-1}$ for 1.8 mM and 5.8 mM, respectively.

3. Results and discussion

3.1. Characterization of rod-shaped colloidal particles

The rod-shaped particles used throughout this project have been prepared by a procedure reported recently[21,22], which was based on a previously reported synthesis of similar particles[35]. The resulting rod-shaped particles consist of silica but have been stabilized by PVP [35]. An example of a typical rod-shaped particle is shown in Fig. 1. The average diameter of the rods was 270 ± 50 nm as determined by scanning electron microscopy imaging (SEM) (cf. Fig. 1a). This diameter range has been confirmed by atomic force microscopy (cf. Fig. 1b). The length of the rods varied from approximately 0.8 μm to 6.6 μm. The rods did show a nearly perfect cylindrical shape, as shown in Fig. 1a and b. However, the surface of the rods showed considerable surface roughness as determined by AFM imaging in Tapping Mode. Fig. 1b shows an AFM-image of a typical rod under ambient conditions. The inset shows the surface topography of the rod after second-order plane fitting. A root-mean-square (RMS) surface roughness in the order of 1.6 nm has been determined, comparable to the roughness typically observed for μm-sized silica colloidal particles synthesized by the Stöber process. For the latter, the RMS-roughness was reported as 2.1 nm [39].

3.2. Preparation of rod probes

One of the major challenges in preparing colloidal probes from rod-shaped colloids was the geometrical constraints that result from the small diameter (*i.e.*, about 300 nm) of the rods. The preparation of colloidal probes, or in this case 'rod probes', on regular, beam-shaped, tipless AFM-cantilevers is not possible due to geometric constraints for most cantilever geometries whose top-view dimensions are not perfectly rectangular but are tapered. Hence, it is geometrically highly probable that the lever arm touches the sample first instead of the rod, due to its small diameter (see Figure S1 in Supplementary Material). Moreover, an additional problem for the preparation of rod probes from rod-shaped colloids on tipless cantilevers arises from the presence of the cantilever beam at a separation distance of less than 1 μm and a tilt angle of 10° for the used AFM. In this case, the large interaction area of the cantilever beam with the substrate cannot be neglected under all conditions, for example, in cases when the interaction is dominated by long-ranged diffuse layer overlap in an electrolyte solution of low ionic strength. Similar considerations concerning the role of the cantilever beam for interaction forces in AFM experiments have been reported previously, albeit for electrostatic interactions [40,41].

So-called plateau tips provide a direct solution to the experimental requirements outlined before (cf. Fig. 2). These tips have only partly the shape of a conventional AFM tip, bearing a plateau at their end instead of an apex. Nevertheless, the tip length before ending in the plateau is several μm. The top-view dimension of the plateau is also in the order of a few μm^2 compared to a sharp tip with a radius of a few nm. Here, commercially available cantilevers with plateau tips have been used [42]. However, the preparation of such tips from standard

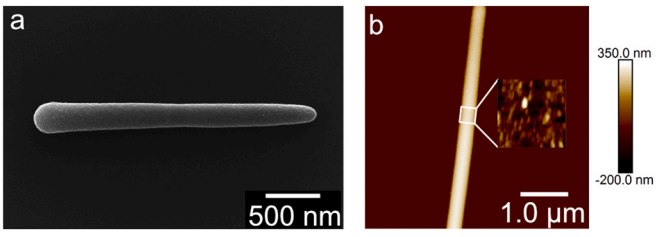

Fig. 1. : (**a**) SEM image of rod-shaped colloid. (**b**) AFM Tapping Mode image of rod-shaped colloid under ambient conditions. The inset is a zoom-in of the surface after 2nd-order plane-fitting and highlights the surface roughness of the rods.

AFM-cantilevers by ablation has also been described previously [43]. Plateau tips find applications, for example, in the field of nano-antenna research [44].

Fig. 2a shows a SEM image of a rod probe prepared from a rod-shaped colloid that has been immobilized to a plateau tip by UV-curable glue. The long axis of the rod has been aligned with the long axis of the cantilever beam. However, other configurations are also possible, such as orthogonal configurations of the long axis. The positioning and immobilization of the rod has been carried out similarly as established for the preparation of spherical colloidal probes[45]. A schematic representation of the different steps involved is given in Figs. 2b and 2c. A small amount of glue has been placed on the plateau tip and subsequently a nanorod was picked up and placed on the droplet of the glue. Essential is here a minimal amount of glue in order to avoid contaminating the rod's surface with glue. The UV-curable glue has been cured under the optical microscope. The resolution of the optical microscope was only sufficient to control the manipulation and alignment but imaging by scanning electron microscopy was necessary in order to exclude the presence of glue on the top surface of rod-shaped particle acting as probe.

3.3. Pre-alignment of rod-shaped particles on substrates

For quantitative direct force measurements, the interaction geometry has to be controlled with a certain degree of accuracy [31,46]. This requirement is even more important for cylindrical objects such as rods, which show more degrees of freedom in the relative orientation. Only accurate alignment of the rods on the sample and cantilever allows for quantitative evaluation, ideally in a crossed-cylinder configuration [9,10,12,13]. Hence, the rods on the substrate should also be pre-aligned, such that ideally, only the substrate has to be aligned. However, the necessary alignment becomes increasingly problematic if the rods are too small to be resolved by optical microscopy: The orientation of the rod on the cantilever is fixed, and in consequence, rods on the substrate have to be identified that show the right orientation (cf. Section 2.4). As this process is time consuming and prone to errors, the pre-alignment of the rods on substrates is advantageous. Moreover, in direct force experiments, one is dealing with low adsorption densities in order to have well-separated, isolated rod-shaped objects. These requirements are similar to the ones well-known from DNA-combing, where DNA is aligned on a substrate, commonly modified mica or glass substrates, by controlling the liquid flow during drying [47–49].

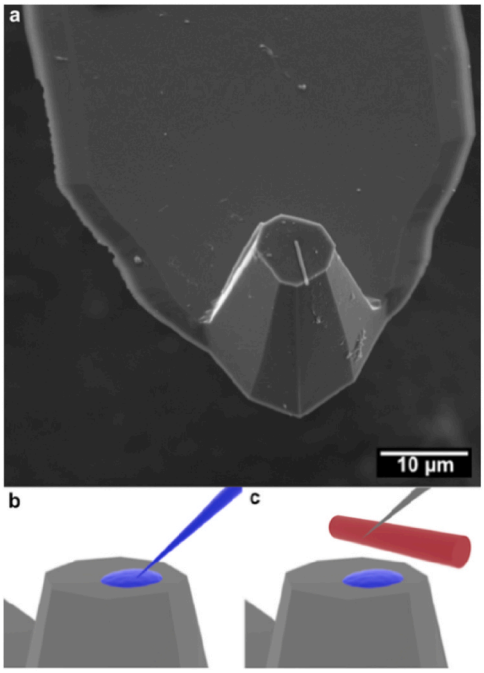

Fig. 2. : (a) SEM image of a rod probe. The rod-shaped silica colloid has been immobilized with a minimal amount of UV-curable glue on the cantilever with plateau tip. (b, c) Schematic representation of the micromanipulation steps for preparing these rod probes: (b) A small amount of UV-curable glue (blue) has been deposited with an etched tungsten wire. (c) The rod-shaped colloid (red) is placed and aligned with another tungsten wire on the plateau tip. Afterwards, UV-curing takes place (not shown).

Here, we followed an approach that resembles important elements of DNA-combing (cf. Fig. 3): A glass substrate has been freshly cleaned by snow-jet treatment, air plasma treatment and by rinsing with ethanol and Milli Q-water, respectively. After cleaning, this substrate has been incubated with a drop of approximately 50 µL of aqueous 0.1 wt% rod suspension. However, the volume depends on the size of the substrate, which should be enough to cover the width of the substrate. The droplet of suspension has been dried immediately under a constant, strong flow of nitrogen (4 bar through a 5 mm nozzle). At this point, a significant part of the liquid has simply been blown away from the surface. In consequence, the resulting density of adsorbed rods is much smaller than for a substrate where the suspension is just allowed to dry. Fig. 4d shows a SEM image demonstrating the resulting pre-alignment of the rods and the resulting low surface coverage.

3.4. Imaging with rod probes

Due to the preferential direction of the rod-shaped colloids on the sample and the pre-defined orientation of the rod fixed on the cantilever, the coarse alignment has been achieved directly by the macroscopic orientation of the sample. However, the final identification of suitable rods on the substrates and the ultimate control of the alignment between the rod probe and sample rod still needs to be controlled. Hence, we chose a direct approach by imaging the substrate with the rod probe as the tip in non-resonant AFM imaging in liquid. Thus, the rod probe is scanned over the sample with adsorbed rods while an AFM-image is acquired. Examples of such images are shown in Fig. 4 for two different orientations between the sample and the rod probe.

The role of tip shape in AFM-imaging has been studied extensively [50,51] even for cantilevers with attached colloidal particles, albeit of spherical shape [52,53]. The surface topography obtained by AFM-imaging results from convolution of the tip and the sample geometry [50,51]. Hence, while imaging with a nanorod-probe is a straightforward procedure, it does not result in high-resolution images (cf. Fig. 4) but is highly dependent on the relative orientation between the rods on the tip and those on the substrate. This effect, resulting from the different convolution by different relative orientations, is used here to ensure a proper alignment between probe and substrate. The difference between the images in Fig. 4a, b and Fig. 4c, d respectively, is evident. For rods aligned in parallel, the convolution in direction of the fast scan axis is minimal (cf. Fig. 4c), while for rods aligned orthogonally, the contact on the fast scan axis (cf. Fig. 4a) lasts for longer periods of time. Hence, in the latter case, we get a 'rectangular'-shaped image of the sample nanorod (cf. Fig. 4b) while in comparison to a 'needle'-like image in the former case (cf. Fig. 4d).

The step outlined in Fig. 4 is essential to ensure the correct relative alignment of the two rods. Imaging with rod probes thus not only allowed for the identification of single rods but also provided necessary confirmation of parallel and crossed cylinder interaction geometry. In Fig. 4b the cross-cylinder interaction geometry has a deviation of approximately $< 10\,\%$ from perfect orthogonality. Moreover, by acquiring the AFM-image, 'point and shoot' force measurements can be conducted. This established technique allows for the exact positioning of the probe on a defined spot of the recently acquired image, using the x-, y-scanner of the AFM in closed-loop feedback. Thereby, measuring interaction forces at well-defined lateral positions of the sample became possible. In Figs. 4b and 4d, positions at which direct force

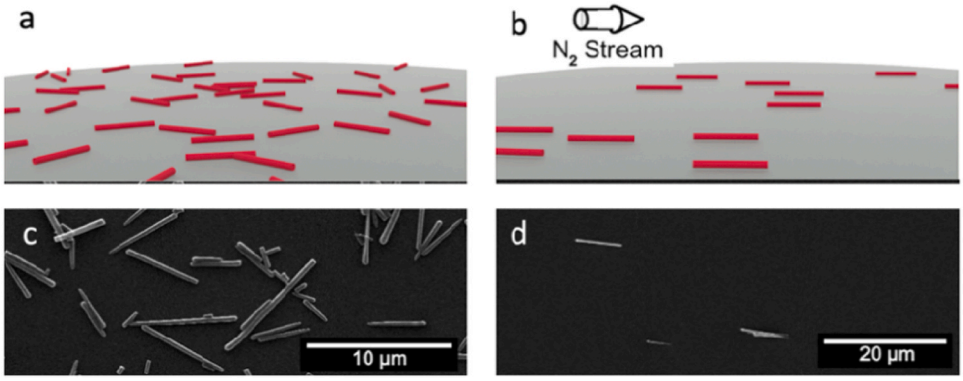

Fig. 3. Comparison of rod orientations after drying without external influence (a, c) and combing by a strong nitrogen stream (b, d). (a) Schematic representation of the rod orientation after drying without external influence and (b) after combing with defined rod orientation. (c) SEM image of the substrate after drying without external influence and (d) after combing.

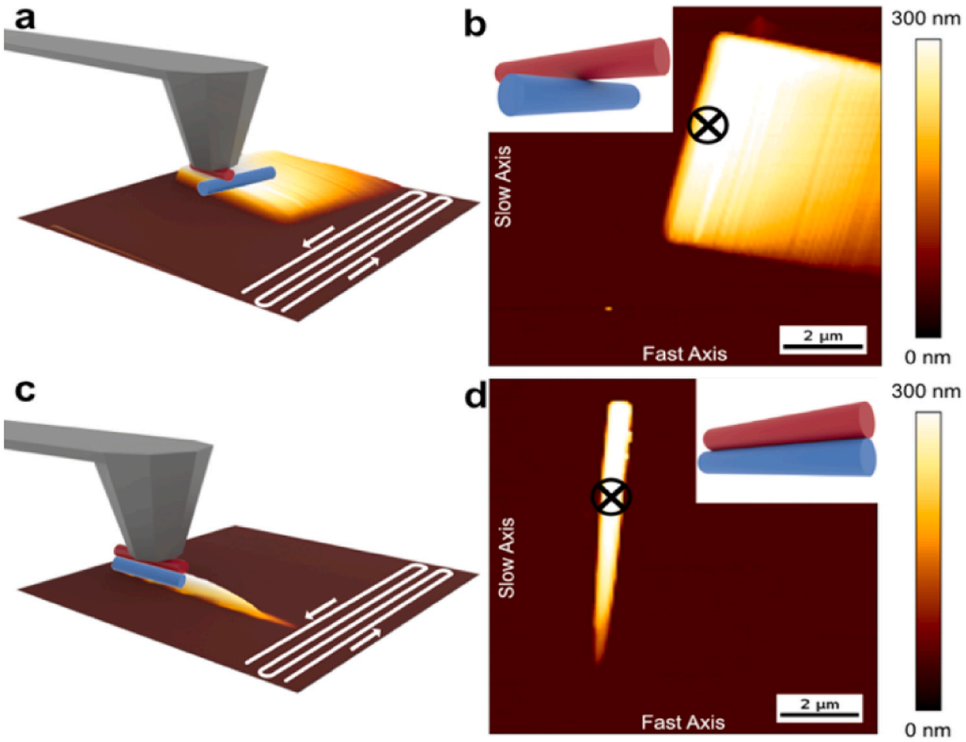

Fig. 4. : Schematic representation for imaging with a rod probe (a, c) and the resulting AFM images (b, d) for crossed cylinder (a, b) and parallel cylinder configurations (c, d). The marks ⊗ in (b) and (d) represent locations at which force-distance curves were subsequently acquired.

measurements in the crossed and parallel cylinder configuration have been indicated by crossed circles. However, in order to identify suitable rods on the substrate with sufficiently high success rate the pre-alignment outlined in 3.3 was necessary.

3.5. Direct force measurements between a pair of aligned rods

Force measurements by AFM allow the relation of the acquired interaction force profiles with surface properties. The Derjaguin approximation provides a direct relation between the measured force $F(D)$ at a given separation D and the free interaction energy per surface area $W(D)$ at the same separation by [33,34,54]:

$$F(D) = 2\pi R_{eff} W(D) \quad (1)$$

The effective radius R_{eff} depends on the interaction geometry. For sphere/sphere interaction, e.g., two colloidal particles with radii R_1 and R_2, we find $R_{eff}^{-1} = R_1^{-1} + R_2^{-1}$. This expression is commonly used for the quantitative evaluation of measurements between two spherical colloids [29–31,46,55,56]. For two perpendicularly crossed cylinders with radii R_1 and R_2, a similar expression can be obtained $R_{eff} = \sqrt{R_1 R_2}$ [33,34]. The latter expression is frequently used to describe experiments by SFA[32,57] and is also the appropriate description of the interaction geometry between two crossed cylinders in AFM-based force measurements [10,12,13]. A theoretical description of the different interaction geometries between to cylinders, i.e., parallel vs. crossed configuration, has been given by Ohshima [58]. In the case of two cylinders interaction in a parallel configuration also the length of the interacting cylinder segments has to be considered.

Fig. 5 shows interaction force profiles that have been acquired between two rod-shaped colloids for two different interaction geometries: In crossed cylinder geometry (cf. Fig. 5a) and parallel cylinder geometry (cf. Fig. 5b), respectively. For each interaction geometry, force profiles

have been acquired in aqueous CsCl-solutions at three different ionic strengths (1.8 mM, 5.8 mM, and 58 mM, respectively). The choice of CsCl as an electrolyte solution has been motivated by the fact that the same electrolyte has been utilized for rheological characterization of suspensions of analogously prepared rod-shaped colloids [22]. The presence of counterions leads to the formation of a diffuse layer of ions at the solid/liquid interface [33]. The characteristic decay constant of the diffuse layer potential due to the increased counterion concentration, respectively, is the so-called Debye length κ^{-1}, which is given by

$$\kappa^{-1} = \sqrt{\frac{\epsilon\epsilon_0 k_B T}{2N_A e^2 I}} \tag{2}$$

where $\varepsilon\varepsilon_0$ is the total permittivity of water, k_BT is the thermal energy at room temperature, N_A is Avogadro's number, e is the elementary charge, and I is the ionic strength, respectively [33].

Here, the ionic strength has been determined by conductometric measurements. The resulting values have been compiled in Table 1. These ionic strengths have been used subsequently to calculate the corresponding theoretical Debye lengths for the different electrolyte solutions; these values are also summarized in Table 1 and can be compared to the experimentally determined Debye lengths as obtained by the fits to the full solutions of the Poisson-Boltzmann equation.

The decay length in the interaction force due to diffuse layer overlap at sufficiently large separation distances can be derived from fits to the interaction force profiles. The free interaction energy between two charged surfaces in an electrolyte solution is approximately proportional to an exponential decay for sufficiently large separations D:

$$W(D) \propto e^{-\kappa D} \tag{3}$$

The exponential decay of Eq. (3) is valid for all sphere/sphere as well as for crossed-cylinder interaction geometries[34]. At smaller separations, *i.e.*, $D < \kappa^{-1}$, effects like charge regulation, surface roughness, and van der Waals force have to be taken into account, and significant deviations from an exponential law are expected [46]. Fig. 5 shows force F versus separation D curves in a semi-logarithmic representation for the different interaction geometries and the three ionic strengths, respectively. In the semi-logarithmic representation, an exponential decay of the interaction forces after Eqs. (1) and (3) will appear as a straight line.

The interaction force profiles for both interaction geometries showed repulsive interaction forces as expected between two identical surfaces (i.e., the rod-shaped silica colloids). The force profiles were mostly linear in the semi-logarithmic representation, except at small separation distances where charge regulation took place. The absence of short-ranged, attractive van-der-Waals (vdW) forces has often been observed for silica-particles and can be attributed to presence of additional steric forces at small separation distances [59–62]. Additional effects include hydration forces [63–65]and surface roughness [46,66]. A similar surface chemistry and surface roughness comparable to silica particles is present for rods.

Table 1
Comparison of Debye lengths derived from conductivity measurements and fits to force profiles.

	Ionic Strength		
	1.8 mM	5.8 mM	58 mM
Theor. Debye length [nm]	7.37	3.99	1.26
Crossed Cylinders [nm]	6.31±2.50	5.19±1.70	2.42±1.45
Parallel Cylinders [nm]	6.20±2.46	4.77±2.04	2.42±1.12

The solid lines in Fig. 5 correspond to fits at large separations of the interaction force profiles. The experimental decay lengths κ^{-1} were extracted from the slope of a linear fit. The fit interval is indicated by the solid lines, whereby the dashed lines represent extrapolations to larger separation distances where the noise due to the thermal movement of the cantilever becomes significant. The results from these fits of the decay constant for the diffuse layer overlap were compiled in Table 1. The experimental errors were determined for $n > 30$ fits to individual force profiles. Additional to the semi-logarithmic representation in Fig. 5 also linear force scale is provide in the supporting information (cf. Figure S3)

The decay lengths, as determined from the interaction force profiles, correspond within the experimental errors to the theoretical Debye lengths calculated from the electrolyte conductivities for both interaction geometries as predicted theoretically [58]. In general, errors are in-line with deviations observed for the direct force measurements on comparable colloidal systems, such as Stöber silica particles [46] and polyelectrolyte-covered silica surfaces [36,67]. We attribute the larger variation at the highest ionic strength to additional non-DLVO forces that are becoming significant at smaller separation distances, which will be discussed later. In general, the interaction force profiles for both interaction geometries are in-line with an interaction that is dominated by diffuse layer overlap and hence the charges present on the rod-shaped particles. However, due to the tilt of the cantilever (cf. Figure S1 in the supporting information) the separation is not completely constant over the whole length of the interacting rod segments, which did lead to increasing deviations at small separations. This effect becomes even more pronounced for the measurement of the interaction profiles

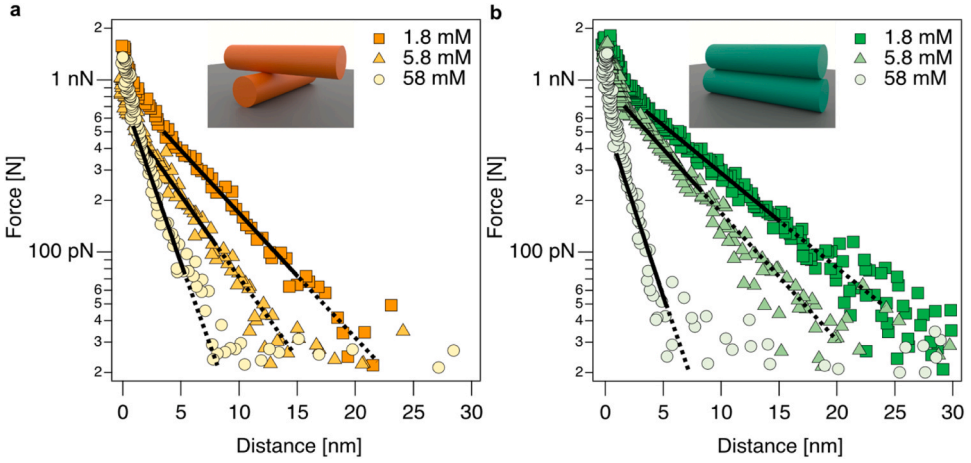

Fig. 5. : Interaction force profiles between two rod-shaped colloids for two different interaction geometries in CsCl solutions of different ionic strength. (a) Crossed cylinder interaction geometry and (b) parallel cylinder interaction geometry. The solid lines represent the fits and fit intervals for the determination of the exponential decay constants. The dashed lines are an extrapolation to larger separation distances.

between the rod-probe and a planar glass surface (cf. Figure S3 c,f,i in the SI). On the other hand the measurements in this interaction geometry confirm the stability of the rod probes.

3.6. Diffuse layer properties of the rod-shaped colloids

The interaction force profiles in Fig. 5a for the crossed-cylinder configuration have been evaluated quantitatively on basis of the Derjaguin approximation [33,54] and have been fitted to the full solutions of the Poisson-Boltzmann (PB) equation, which describes the forces due to the overlap of the diffuse layers [27,68]. A quantitative evaluation of the interaction force profiles for the parallel cylinder configuration would demand an accurate knowledge about the segment lengths that were involved in the interaction [58]. Moreover, due to the tilt of the cantilever the separation would be not constant. Hence, this approach has been not followed here and we did concentrate on the crossed cylinder geometry.

Fig. 6 shows the interaction force profiles for I=1.8 mM and I=5.8 mM, respectively, with the corresponding fits to the PB-equation. Besides the two well-known boundary conditions of constant charge (CC) and constant potential (CP) [33,54], we also included charge regulation on the basis of the constant regulation (CR) approximation [38]. This approximation summarizes all contributions from ionizable groups at the surface by means of a regulation parameter p that can be expressed as the ratio of the inner surface capacitance C_i and the diffuse layer capacitance C_{dl}. The classical boundary conditions correspond to p=0 (CP) and p=1 (CC), respectively. The constant regulation approximation has been successfully applied to inorganic surfaces [38,69] as well as adsorbed polyelectrolyte layers [36,67]. The fits in Fig. 6 result from p=0.6, which is compatible with charge regulation for silica colloidal particles [69] as well as polyelectrolyte layers [36,67]. However, the good agreement of the fits for all three boundary conditions at separation distances larger than one Debye length indicates that the diffuse layer potentials ψ^{dl} reported in Fig. 7, which were obtained at separation distances $\kappa^{-1}<D<2\kappa^{-1}$, are basically independent of the boundary conditions (CC, CP, and CR) in the evaluated interval.

Fig. 7a,b summarize the results for ψ^{dl} as obtained from the fits for the two lowest ionic strengths, namely 1.8 mM and 5.8 mM, for various sequences of direct force measurements. The data shown in Fig. 7a originate from force profiles acquired at various positions (Pos. 1–3 and Pos. 1–4, respectively) for two different rods but always acquired with the same rod probe. Within one position, the values for the diffuse layer potentials show only small variations, while the values for ψ^{dl} change noticeably between the different positions on the same rod. However,

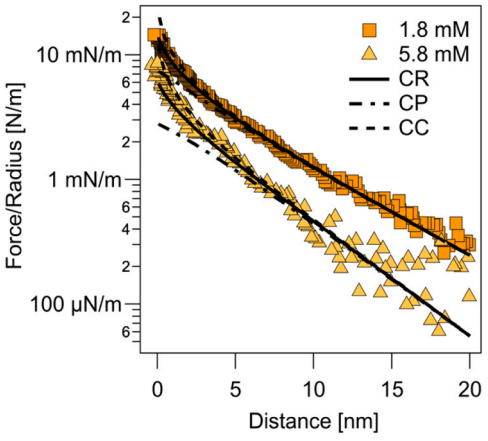

Fig. 6. : Interaction force profiles between two rod-shaped colloids in the crossed cylinder geometry. The dashed lines indicate fits to the constant charge (CC) and constant potential (CP) boundary conditions, respectively. The solid lines indicate fits, including charge regulation (CR) (p=0.6).

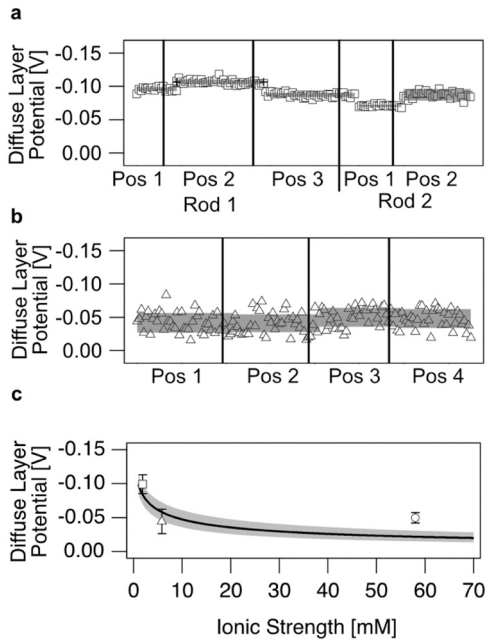

Fig. 7. : (a) Diffuse layer potentials for different positions on two different immobilized rods in the crossed cylinder geometry and I=1.8 mM CsCl. (b) Diffuse layer potentials for different positions on rods in crossed cylinder geometry and I=5.8 mM CsCl. **(c)** Diffuse layer potential versus ionic strength. The solid line is the extrapolation according to the Grahame equation for the values at 1.8 mM. The error bars of the diffuse layer potentials as obtained from the fits to the Poisson-Boltzmann equation correspond to their standard deviation from all performed fits.

the variations between different positions and different rods seem to be comparable. The observed variation in the diffuse layer potentials can be attributed primarily to various effects: (i) significant surface charge heterogeneities on the rods. (ii) Local variations in the surface roughness of the interaction area on both rod-shaped particles. (iii) Variations of the rod diameter of the rods, respectively. The latter contribution would be possible according to the SEM images (cf. Fig. 1a) but might not be sufficient to explain the full scale of variations observed. Hence, we suggest that all three effects contributed to the observed variation.

Fig. 7b shows diffuse layer potentials from fits to force profiles acquired at I=5.8 mM on different positions of the same rod. Due to the smaller Debye lengths at this higher ionic strength, the surface roughness of the rods (cf. Fig. 1b) does exert a larger influence as the diffuse layer potentials have been determined at smaller separation distances. Hence, the scattering of the data for one position increased significantly as small lateral variation due to drift contributed more. Nevertheless, also for 5.8 mM a difference at different positions can be observed for ψ^{dl}, as can be seen for the averaged values for each position (see shaded areas in Fig. 7b).

The diffuse layer potentials ψ^{dl} determined here for the rod-shaped colloids are much higher than the ones normally reported for Stöber silica particles under equal conditions. [63–66,70,71] Here, ψ^{dl} =-99.2 ±7.9 mV at 1.8 mM have been derived for the rod-shaped colloids in comparison to a value range of −45 mV to −60 mV in a similar pH-regime for spherical Stöber silica particles [63–66,70,71]. Analysis of the diffuse layer potentials ψ^{dl} vs. ionic strength I by means of the Grahame equation indicates a much higher charge density for the rod-shaped colloids than commonly reported for spherical silica particles. The Grahame equation relates the charge density σ with the diffuse layer potential ψ^{dl} by

$$\sigma = \sqrt{8I\epsilon\epsilon_0 RT}\sinh\left(\frac{F\psi^{dl}}{2RT}\right) \quad (4)$$

with F as the Faraday constant and R as the universal gas constant, respectively. Fig. 7c shows the diffuse layer potentials ψ^{dl} as a function of the ionic strength I, with the solid line being the extrapolation of the Grahame equation for $\psi^{dl} = -99.2 \pm 7.9$ mV at 1.8 mM, which corresponds to a charge density of $\sigma = -12.7$ mC/m^2. This charge density is rather high compared to $\sigma = -6.1$ mC/m^2 for 'classical' Stöber silica particles[62]. The shaded area in Fig. 7c shows the error propagation for the charge density $\sigma = -12.7$ mC/m^2. While the diffuse layer potential at I=5.8 mM did fall well within the range given by this error propagation, the diffuse layer potentials at I=58 mM are clearly much higher than expected on basis of the Grahame equation. However, the large deviation between the experimental and the theoretical value of the Debye length at 58 mM supports the interpretation of additional steric forces. Such steric forces have been primarily observed for polyelectrolyte layers [36,67] but have also been reported for silicic acid hairs [59]. Such steric force can be rather extended and can be described approximately by the Alexander-de Gennes theory for polyelectrolytes [72]. However, here, a flatter adsorption conformation than the one of a brush must be assumed with an extension of only a few nm [73–75]. It should be noted that despite the use of the polyelectrolyte polyvinylpyrrolidone (PVP) in the synthesis of the rod-shaped silica particles, a polyelectrolyte layer would result in a reduced charge density or charge reversal. The latter can be excluded as interaction forces between the rod-probe and the glass substrate were repulsive (data not shown). Moreover, much lower absolute charge densities in the range of $\sigma = 2.3$ mC/m^2[36] – 1.5 mC/m^2 [67] for silica surfaces completely covered with adsorbed polycations have been observed. Hence, the most likely explanation for the high surface charge density is a layer of silicidic acid hairs. Similar effects of increased surface charge density due to increased volume charge density due to surface porosity have been reported for silica particles [76–78]. The presence of a porous layer and silicidic acid hairs on the here-prepared could be verified by heat-treatment, i.e., a type of calcination, which would result in a reduction in porosity as reported for Stöber silica particles [78].

4. Conclusions

Here, we report for the first time a proof-of-concept for direct force measurements between rod-shaped colloids with diameters of a few hundred nanometers. The here-developed approach allows to extend quantitative direct force measurements in a defined interaction geometry for colloidal objects that cannot be resolved properly by optical microscopy anymore. Quantitative evaluation of the resulting interaction force profiles can be accomplished in the crossed-cylinder geometry in the framework of the Derjaguin approximation and a comparison to the DLVO-theory can be performed. Hence, one of the greatest advantages of the colloidal probe technique, measuring the interaction forces between real colloidal objects rather than model systems, can now also be utilized for rod-shaped colloidal particles. However, it should be kept in mind that due to the small radii of curvature, the absolute forces are smaller compared to 'classical' spherical colloidal probes in the micrometer range [36,46,55,69] and are comparable to sub-micrometer spherical colloidal probes [25,29–31,56,79]. By utilizing cantilevers with the same type of plateau tips but lower spring constants and an additional reflective coating, the experimental force sensitivity could be increased significantly if necessary.

Our results show that the rod-shaped silica colloids, as used in recent studies [21,22] bear a surface charge that is much higher than expected. Hence, approximations of the interaction potentials based on data for silica particles synthesized by the Stöber process [63–66,70,71] would be misleading. One rationalization for the higher charge densities here would be an increased volume charge density with protruding silicidic acid hairs, as also observed for Stöber silica under certain conditions [59]. In future works, this question could be answered by applying heat-treatment as demonstrated by Kobayashi et al. [78] as well as performing electrophoretic mobility measurements where the Smoluchowski approximation would be valid also for the rod-shaped particles. Due to the isotropic nature of the rod-shaped particles, we assume that there might also be a significant charge density difference between the lateral surface and the tip of the rods. This assumption stems from observing rod aggregation in the dilute regime where the tendency is always a cross configuration and not tip-to-tip, body-to-tip, or parallel configuration. However, for large separation distances, the interaction force profiles are clearly compatible with DLVO theory as indicated by the Debye-lengths irrespectively of the orientation. Therefore, interaction forces due to surface charge play a significant role at low ionic strengths.

Generally, the presence of heterogenous charge distributions, surface roughness, and adsorbed polymeric layers often make the modeling of real-world colloidal systems difficult and require the actual experimental determination of interaction profiles and adhesion forces, respectively. Our example demonstrates insights that might provide urgently needed information to model such systems, for example, in terms of their rheological properties [21,22]. Other fields of application might be, for example, adsorption studies where the inter-particle interaction potentials are of great relevance, such as RSA-models for non-spherical colloids [23,24]. Along these lines, future studies involving frictional measurements of rod-like colloids approached at different relative angles would be valuable for understanding the micromechanics and, eventually, the structure formation and mechanical response of rod-like particle colloidal gels [21,22,80].

Funding

This work has received funding from the European Union's Horizon 2020 research and innovation program under grant agreement No 731019 (EUSMI).

The authors also acknowledge support by the Elite Network of Bavaria (ENB) through the study program "Macromolecular Science". The authors acknowledge support by the University of Bayreuth Graduate School.

Declaration of Competing Interest

The authors declare that they have no known competing financial interests or personal relationships that could have appeared to influence the work reported in this paper.

Data availability

Data will be made available on request.

Acknowledgements

The authors are indebted to Paul Markus for help with the programming and Carmen Kunert for help with the electron microscopy. We also thank Lucille Chambon and Maria Vamvakaki (IESL, FORTH) for the synthesis of the silica rods.

Appendix A. Supporting information

Supplementary data associated with this article can be found in the online version at doi:10.1016/j.colsurfa.2024.134319.

References

[1] H.J. Butt, M. Jaschke, Calculation of thermal noise in atomic force microscopy, Nanotechnology 6 (1995) 1–7, https://doi.org/10.1088/0957-4484/6/1/001.
[2] H.-J. Butt, B. Cappella, M. Kappl, Force measurements with the atomic force microscope: technique, interpretation and applications, Surf. Sci. Rep. 59 (2005) 1–152, https://doi.org/10.1016/j.surfrep.2005.08.003.

[3] W.A. Ducker, T.J. Senden, R.M. Pashley, Direct measurement of colloidal forces using an atomic force microscope, Nature 353 (1991) 239–241, https://doi.org/10.1038/353239a0.

[4] H.-J. Butt, Measuring electrostatic, van der Waals, and hydration forces in electrolyte solutions with an atomic force microscope, Biophys. J. 60 (1991) 1438–1444, https://doi.org/10.1016/s0006-3495(91)82180-4.

[5] M. Kappl, H. Butt, The colloidal probe technique and its application to adhesion force measurements, Part. Part. Syst. Charact.: Meas. Descr. Part. Prop. Behav. Powders Other Disperse Syst. 19 (2002) 129–143, https://doi.org/10.1002/1521-4117(200207)19.

[6] Y. Gan, Invited Review Article: a review of techniques for attaching micro- and nanoparticles to a probe's tip for surface force and near-field optical measurements, Rev. Sci. Instrum. 78 (2007) 081101, https://doi.org/10.1063/1.2754076.

[7] C.C. Yuan, D. Zhang, Y. Gan, Invited Review Article: tip modification methods for tip-enhanced Raman spectroscopy (TERS) and colloidal probe technique: a 10 year update (2006-2016) review, Rev. Sci. Instrum. 88 (2017) 031101, https://doi.org/10.1063/1.4978929.

[8] N. Helfricht, et al., Probing the adhesion properties of alginate hydrogels: a new approach towards the preparation of soft colloidal probes for direct force measurements, Soft Matter 13 (2017) 578–589, https://doi.org/10.1039/c6sm02326f.

[9] L. Meagher, et al., Interaction forces between α-alumina fibres in aqueous electrolyte measured with an atomic force microscope, Colloids Surf. A-Physicochem. Eng. Asp. 146 (1999) 123–137, https://doi.org/10.1016/s0927-7757(98)00779-1.

[10] I. Muir, L. Meagher, M. Gee, Interaction forces between alpha-alumina fibers with coadsorbed polyelectrolyte and surfactant, Langmuir 17 (2001) 4932–4939, https://doi.org/10.1021/la010045t.

[11] A. Elbourne, et al., Adsorbed and near-surface structure of ionic liquids determines nanoscale friction, Chem. Commun. 49 (2013) 6797, https://doi.org/10.1039/c3cc42844c.

[12] B.R. Neugirg, et al., Long-range interaction forces between 1,3,5-cyclohexanetrisamide fibers in crossed-cylinder geometry, Polymer 102 (2016) 363–371, https://doi.org/10.1016/j.polymer.2016.03.068.

[13] K. Sato, et al., A feasibility study on direct measurements of interaction forces between carbon fiber surfaces and other substances, Polym. Compos. 41 (2020) 5209–5215, https://doi.org/10.1002/pc.25787.

[14] N. Ma, et al., Programmable interactions of cellulose acetate with octadecyltrichlorosilane-functionalized SiO2 nanoparticles, Langmuir 39 (2023) 5956–5969, https://doi.org/10.1021/acs.langmuir.2c03232.

[15] T. Wang, et al., Microstructural probing of phosphonium-based ionic liquids on a gold electrode using colloid probe AFM, Phys. Chem. Chem. Phys. 24 (2022) 25411–25419, https://doi.org/10.1039/d2cp02489f.

[16] Y. Wei, et al., Molecular interactions of ionic liquids with SiO2 surfaces determined from colloid probe atomic force microscopy, Phys. Chem. Chem. Phys. 24 (2022) 12808–12815, https://doi.org/10.1039/d2cp00483f.

[17] Y. Wei, et al., Detailing molecular interactions of ionic liquids with charged SiO2 surfaces: A systematic AFM study, J. Mol. Liq. 350 (2022) 118506, https://doi.org/10.1016/j.molliq.2022.118506.

[18] J.K.G. Dhont, W.J. Briels, Viscoelasticity of suspensions of long, rigid rods, Colloids Surf. A: Physicochem. Eng. Asp. 213 (2003) 131–156, https://doi.org/10.1016/s0927-7757(02)00508-3.

[19] M.J. Solomon, P.T. Spicer, Microstructural regimes of colloidal rod suspensions, gels, and glasses, Soft Matter 6 (2010) 1391, https://doi.org/10.1039/b918281k.

[20] M. Wittmann, et al., Rod-shaped microparticles — an overview of synthesis and properties, Colloid Polym. Sci. 301 (2023) 783–799, https://doi.org/10.1007/s00396-023-05111-3.

[21] L. Chambon, et al., Colloidal rod-like particles with temperature-driven tunable interactions, Langmuir 38 (2022) 13674–13685, https://doi.org/10.1021/acs.langmuir.2c01716.

[22] M. Das, G. Petekidis, Shear induced tuning and memory effects in colloidal gels of rods and spheres, J. Chem. Phys. 157 (2022), https://doi.org/10.1063/5.0129709.

[23] Z. Adamczyk, et al., QCM-D investigations of anisotropic particle deposition kinetics: evidences of the hydrodynamic slip mechanisms, Anal. Chem. 94 (2022) 10234–10244, https://doi.org/10.1021/acs.analchem.2c01776.

[24] M. Morga, et al., Mechanisms of anisotropic particle deposition: prolate spheroid layers on mica, J. Phys. Chem. C. 126 (2022) 18550–18559, https://doi.org/10.1021/acs.jpcc.2c06028.

[25] C.-P. Hsu, et al., Roughness-dependent tribology effects on discontinuous shear thickening, Proc. Natl. Acad. Sci. 115 (2018) 5117–5122, https://doi.org/10.1073/pnas.1801066115.

[26] H.-J. Butt, et al., Impact of atomic force microscopy on interface and colloid science, Adv. Colloid Interface Sci. 133 (2007) 91–104, https://doi.org/10.1016/j.cis.2007.06.001.

[27] M. Borkovec, et al., Investigating forces between charged particles in the presence of oppositely charged polyelectrolytes with the multi-particle colloidal probe technique, Adv. Colloid Interface Sci. 179-182 (2012) 85–98, https://doi.org/10.1016/j.cis.2012.06.005.

[28] M. Auffan, et al., Towards a definition of inorganic nanoparticles from an environmental, health and safety perspective, Nat. Nanotechnol. 4 (2009) 634–641, https://doi.org/10.1038/nnano.2009.242.

[29] F.J. Montes Ruiz-Cabello, et al., Electric double-layer potentials and surface regulation properties measured by colloidal-probe atomic force microscopy, Phys. Rev. E 90 (2014), https://doi.org/10.1103/physreve.90.012301.

[30] N. Helfricht, et al., Extending the limits of direct force measurements: colloidal probes from sub-micron particles, Nanoscale 9 (2017) 9491–9501, https://doi.org/10.1039/c7nr02226c.

[31] A. Mark, et al., The next generation of colloidal probes: a universal approach for soft and ultra-small particles, Small 15 (2019) 1902976, https://doi.org/10.1002/smll.201902976.

[32] J. Israelachvili, et al., Recent advances in the surface forces apparatus (SFA) technique, Rep. Prog. Phys. 73 (2010) 036601–036616, https://doi.org/10.1088/0034-4885/73/3/036601.

[33] J. Israelachvili, Intermolecular and Surface Forces, Academic Press, 2011.

[34] J. Zhang, H. Zeng, Intermolecular and surface interactions in engineering processes, Engineering 7 (2021) 63–83, https://doi.org/10.1016/j.eng.2020.08.017.

[35] A. Kuijk, A. van Blaaderen, A. Imhof, Synthesis of Monodisperse, Rodlike Silica Colloids with Tunable Aspect Ratio, J. Am. Chem. Soc. 133 (2011) 2346–2349, https://doi.org/10.1021/ja109524h.

[36] R. Pericet-Camara, et al., Interaction forces and molecular adhesion between pre-adsorbed poly(ethylene imine) layers, J. Colloid Interface Sci. 296 (2006) 496–506, https://doi.org/10.1016/j.jcis.2005.09.033.

[37] J.L. Hutter, J. Bechhoefer, Calibration of atomic-force microscope tips, Rev. Sci. Instrum. 64 (1993) 1868–1873, https://doi.org/10.1063/1.1143970.

[38] R. Pericet-Camara, et al., Interaction between charged surfaces on the poisson−boltzmann level: the constant regulation approximation, J. Phys. Chem. B 108 (2004) 19467–19475, https://doi.org/10.1021/jp0473063.

[39] V. Kuznetsov, G. Papastavrou, Adhesion of colloidal particles on modified electrodes, Langmuir 28 (2012) 16567–16579, https://doi.org/10.1021/la3029726.

[40] S. Guriyanova, D.S. Golovko, E. Bonaccurso, Cantilever contribution to the total electrostatic force measured with the atomic force microscope, Meas. Sci. amp; Technol. 21 (2010) 025502, https://doi.org/10.1088/0957-0233/21/2/025502.

[41] S. Bradler, et al., A theoretical model for the cantilever motion in contact-resonance atomic force microscopy and its application to phase calibration in piezoresponse force and electrochemical strain microscopy, J. Appl. Phys. 120 (2016) 165107, https://doi.org/10.1063/1.4964942.

[42] R.G. Dixson, N.G. Orji, R.S. Goldband, Lateral tip control effects in critical dimension atomic force microscope metrology: the large tip limit, J. Micro/Nanolithogr., MEMS, MOEMS 15 (2016) 014003, https://doi.org/10.1117/1.jmm.15.1.014003.

[43] P. Biagioni, et al., A simple method for producing flattened atomic force microscopy tips, Rev. Sci. Instrum. 79 (2008), https://doi.org/10.1063/1.2834875.

[44] P. Biagioni, J.-S. Huang, B. Hecht, Nanoantennas for visible and infrared radiation, Rep. Prog. Phys. 75 (2012) 024402, https://doi.org/10.1088/0034-4885/75/2/024402.

[45] V. Kuznetsov, G. Papastavrou, Note: mechanically and chemically stable colloidal probes from silica particles for atomic force microscopy, Rev. Sci. Instrum. 83 (2012) 116103, https://doi.org/10.1063/1.4765299.

[46] S. Rentsch, et al., Probing the validity of the Derjaguin approximation for heterogeneous colloidal particles, Phys. Chem. Chem. Phys. 8 (2006) 2531, https://doi.org/10.1039/b602145j.

[47] D. Bensimon, et al., Stretching DNA with a receding meniscus: experiments and models, Phys. Rev. Lett. 74 (1995) 4754–4757, https://doi.org/10.1103/physrevlett.74.4754.

[48] A. Benke, M. Mertig, A. Pompe, PH- and salt-dependent molecular combing of DNA: experiments and phenomenological model, Nanotechnology 22 (2011), https://doi.org/10.1088/0957-4484/22/3/035304.

[49] Z. Esmail Nazari, L. Gurevich, Controlled deposition and combing of DNA across lithographically defined patterns on silicon, Beilstein J. Nanotechnol. 4 (2013) 72–76, https://doi.org/10.3762/bjnano.4.8.

[50] J.S. Villarrubia, Algorithms for scanned probe microscope image simulation, surface reconstruction, and tip estimation, J. Res. Natl. Inst. Stand. Technol. 102 (1997) 425–454, https://doi.org/10.6028/jres.102.030.

[51] J. Canet-Ferrer, et al., Correction of the tip convolution effects in the imaging of nanostructures studied through scanning force microscopy, Nanotechnology 25 (2014) 395703, https://doi.org/10.1088/0957-4484/25/39/395703.

[52] C. Neto, V.S.J. Craig, Colloid probe characterization: radius and roughness determination, Langmuir 17 (2001) 2097–2099, https://doi.org/10.1021/la001506y.

[53] L. Kain, et al., Calibration of colloidal probes with atomic force microscopy for micromechanical assessment, J. Mech. Behav. Biomed. Mater. 85 (2018) 225–236, https://doi.org/10.1016/j.jmbbm.2018.05.026.

[54] H. Butt, K. Graf, M. Kappl, Physics and chemistry of interfaces, Wiley, 2003.

[55] I. Popa, et al., Importance of charge regulation in attractive double-layer forces between dissimilar surfaces, Phys. Rev. Lett. 104 (2010) 228301, https://doi.org/10.1103/PhysRevLett.104.228301.

[56] F.J.M. Ruiz-Cabello, et al., Forces between different latex particles in aqueous electrolyte solutions measured with the colloidal probe technique, Microsc. Res. Tech. 80 (2017) 144–152, 10.1002/jemt.22656.

[57] P.M. Claesson, et al., Techniques for measuring surface forces, Adv. Colloid Interface Sci. 67 (1996) 119–183, https://doi.org/10.1016/0001-8686(96)00302-8.

[58] H. Ohshima, Approximate analytic expressions for the electrostatic interaction energy between two colloidal particles based on the modified Poisson-Boltzmann equation, Colloid Polym. Sci. 295 (2017) 289–296, https://doi.org/10.1007/s00396-016-4005-5.

[59] G. Vigil, et al., Interaction of silcia surfaces, J. Colloid Interface Sci. 165 (1994) 367–385, https://doi.org/10.1006/jcis.1994.1242.
[60] M. Kobayashi, et al., Effects of heat treatment on the aggregation and charging of Stober-type silica, J. Colloid Interface Sci. 292 (2005) 139–147, https://doi.org/10.1016/j.jcis.2005.05.093.
[61] S.M. Acuña, P.G. Toledo, Short-range forces between glass surfaces in aqueous solutions, Langmuir 24 (2008) 4881–4887, https://doi.org/10.1021/la703866g.
[62] V. Valmacco, et al., Forces between silica particles in the presence of multivalent cations, J. Colloid Interface Sci. 472 (2016) 108–115, https://doi.org/10.1016/j.jcis.2016.03.043.
[63] J.J. Valle-Delgado, et al., Hydration forces between silica surfaces: Experimental data and predictions from different theories, J. Chem. Phys. 123 (2005) 034708, https://doi.org/10.1063/1.1954747.
[64] M. Dishon, O. Zohar, U. Sivan, From repulsion to attraction and back to repulsion: the effect of NaCl, KCl, and CsCl on the force between silica surfaces in aqueous solution, Langmuir 25 (2009) 2831–2836, https://doi.org/10.1021/la803022b.
[65] J. Morag, M. Dishon, U. Sivan, The governing role of surface hydration in ion specific adsorption to silica: an AFM-based account of the hofmeister universality and its reversal, Langmuir 29 (2013) 6317–6322, https://doi.org/10.1021/la400507n.
[66] R.F. Considine, C.J. Drummond, Surface roughness and surface force measurement: a comparison of electrostatic potentials derived from atomic force microscopy and electrophoretic mobility measurements 17 (2001) 7777–7783, https://doi.org/10.1021/la0017227.
[67] L.J. Kirwan, et al., Interaction and structure of surfaces coated by poly(vinyl amines) of different line charge densities, J. Phys. Chem. B 112 (2008) 14609–14619, https://doi.org/10.1021/jp802366p.
[68] A.M. Smith, M. Borkovec, G. Trefalt, Forces between solid surfaces in aqueous electrolyte solutions, Adv. Colloid Interface Sci. 275 (2020) 102078, https://doi.org/10.1016/j.cis.2019.102078.
[69] V. Kuznetsov, G. Papastavrou, Ion adsorption on modified electrodes as determined by direct force measurements under potentiostatic control, J. Phys. Chem. C. 118 (2014) 2673–2685, https://doi.org/10.1021/jp500425g.
[70] P.G. Hartley, I. Larson, P.J. Scales, Electrokinetic and direct force measurements between silica and mica surfaces in dilute electrolyte solutions, Langmuir 13 (1997) 2207–2214, https://doi.org/10.1021/la960997c.
[71] R.G. Horn, D.T. Smith, W. Haller, Surface forces and viscosity of water measured between silica sheets, Chem. Phys. Lett. 162 (1989) 404–408, https://doi.org/10.1016/0009-2614(89)87066-6.
[72] S. Block, C.A. Helm, Measurement of long-ranged steric forces between polyelectrolyte layers physisorbed from 1 M NaCl, Phys. Rev. E 76 (2007) 030801, https://doi.org/10.1103/PhysRevE.76.030801.
[73] L.M. Al-Harbi, et al., Adsorption of polyvinylpyrrolidone over the silica surface: as affected by pretreatment of adsorbent and molar mass of polymer adsorbate, Int. J. Polym. Sci. 2016 (2016) 1–9, https://doi.org/10.1155/2016/2417292.
[74] K. Esumi, M. Oyama, Simultaneous adsorption of poly(vinylpyrrolidone) and cationic surfactant from their mixed solutions on silica, Langmuir 9 (1993) 2020–2023, https://doi.org/10.1021/la00032a021.
[75] V.M. Gun'ko, et al., Adsorption and migration of poly(vinyl pyrrolidone) at a fumed silica surface, Adsorpt. Sci. Technol. 24 (2006) 143–158, https://doi.org/10.1260/026361706778529173.
[76] A. de Keizer, E.M. van der Ent, L.K. Koopal, Surface and volume charge densities of monodisperse porous silicas, Colloids Surf. A-Physicochem. Eng. Asp. 142 (1998) 303–313, https://doi.org/10.1016/S0927-7757(98)00268-4.
[77] M. Minor, et al., Streaming potentials and conductivities of porous silica plugs, Colloids Surf. A: Physicochem. Eng. Asp. 142 (1998) 165–173, https://doi.org/10.1016/s0927-7757(98)00365-3.
[78] M. Kobayashi, et al., Aggregation and charging of colloidal silica particles: effect of particle size, Langmuir 21 (2005) 5761–5769, https://doi.org/10.1021/la046829z.
[79] P. Sinha, et al., Attractive forces between charged colloidal particles induced by multivalent ions revealed by confronting aggregation and direct force measurements, J. Phys. Chem. Lett. 4 (2013) 648–652, https://doi.org/10.1021/jz4000609.
[80] M. Das, et al., Shear driven vorticity aligned flocs in a suspension of attractive rigid rods, Soft Matter 17 (2021) 1232–1245, https://doi.org/10.1039/d0sm01576h.